2020 IEEE Latin America Electron Devices Conference (LAEDC)
San José, Costa Rica, February 25-28, 2020

Dynamic Response Considerations in Typical CMOS-MEMS Accelerometer Structures

Benito Granados-Rojas, *Member, IEEE,* Mario A. Reyes-Barranca, Griselda S. Abarca-Jiménez, and Yesenia E. González-Navarro

Abstract — **This work presents important considerations regarding the dynamic response of a CMOS-MEMS spring-mass-system to step (Heaviside) and ramp (linear input) force stimuli. In the design CMOS-MEMS accelerometers most performance estimations and calculations are based in the steady-state behavior of damped systems, the present report focuses in the transient response and oscillatory error due to external forces actually present in many real-world yet simple applications where vibrations and undesired disturbances might appear. The dynamic model and transfer function of a micro-spring-mass system is obtained according to the technological fabrication parameters of a typical CMOS-MEMS micro-sensor. The displacement and therefore capacitance shift of the micro-structure is modeled and simulated primarily while neglecting gravity and the damping phenomena related to air-filled micro gaps inherent to the micro-machining (wet chemical) process needed to release movable metallic structures out of a conventional CMOS integrated circuit. The results are intended to be considered in the design of space applications such as spacecraft instrumentation.**

Index Terms — **Accelerometer, CMOS-MEMS, Dynamic Model, Mechanical Model, MEMS, Step Response.**

I. Introduction

THE technology known as CMOS-MEMS combines in a single chip (silicon die) the capabilities of both CMOS conventional circuitry and the electromechanical micro-devices and structures (MEMS). When it comes to inertial sensors, the basic micro-structure used to measure acceleration is a mass-spring-system-like mechanism coupled to a variable capacitor which capacitance value varies proportionally to the displacement of the proof-mass. As this proof-mass approaches closer to another also metallic plate the capacitance given by (1), the parallel plate capacitor, increases. Parallel plate capacitance is proportional to the plate area A, the electric permittivity ϵ_0 (air or vacuum), and the inverse of the gap d between plates. The relation between the mass-spring system displacement and the variable capacitor is shown in Fig. 1.

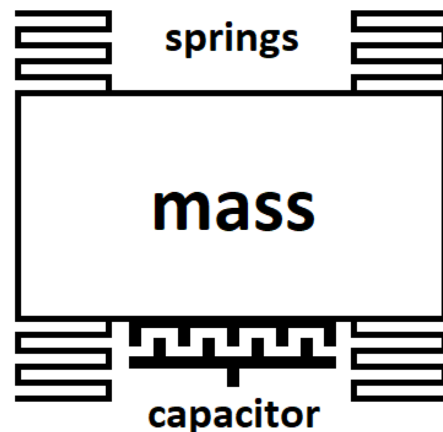

Fig. 1. Schematic for a typical mass-spring-system-based CMOS-MEMS accelerometer featuring a main proof-mass attached to four springs.

$$C = \epsilon_0 A/d \tag{1}$$

As seen in [1] capacitors might not be simple plates but complex tridimensional structures with many capacitive components, nevertheless, neglecting fringe effects, the approximation for total capacitance is quite fair.

CMOS-MEMS process consists in having a previously designed and fabricated conventional CMOS chip where the electronic control/processing circuitry coexist along with one or more metal patterns, and release the later in order to achieve full electromechanical functions. As expected, these metallic structures are made out of the metal layers intended to interconnect devices as usual in any CMOS integrated circuits. As reported in [2] the composition and thicknesses of these metal layers varies according to the fabrication process as some processes feature TiN platting on their metal pathways for contact improvement purposes. However, an aluminum-copper alloy can be found in most conventional CMOS fabrication technologies. Since copper is typically under 5% in concentration, the calculation for density and stiffness in this report are based in the aluminum mechanical properties.

Support from CONACyT through Ph.D. scholarship 295930 granted to Benito Granados-Rojas is gratefully acknowledged.

B. Granados-Rojas and M. A. Reyes-Barranca are with Sección de Electrónica del Estado Sólido, CINVESTAV, 07360, Mexico (e-mail: bgranadosr@cinvestav.mx , mreyes@cinvestav.mx).

G. S. Abarca-Jiménez is with Academia de Ciencias de la Ingeniería, UPIIH, Instituto Politécnico Nacional, 42162, Mexico (e-mail: gabarcaj@ipn.mx).

Y. E. González-Navarro is with Departamento de Ingeniería, UPIITA, Instituto Politécnico Nacional, 07340, Mexico (e-mail: ygonzalezn@ipn.mx).

978-1-7281-1044-8/20/$31.00 ©2020 IEEE

Authorized licensed use limited to: CINVESTAV. Downloaded on August 07,2020 at 18:23:45 UTC from IEEE Xplore. Restrictions apply.

Each one of the four springs considered in the schematic seen above is formed by a series of multiple aluminum beams, every beam can be modeled in a similar way to that proposed by Hook's Law in (2), in order to determine the equivalent stiffness k of a particular beam of length L it is useful to apply the cantilever deflection expressions (3) for a given Young's Modulus E and inertia momentum I when a load force P is actuating on the free end.

$$F = kx$$

$$k = \frac{F}{x} \tag{2}$$

$$\delta_{beam} = \frac{PL^3}{3EI} \tag{3}$$

Figure 2 represents the analogy between traditional coil-like and cantilever springs. Must be also considered the effect of having multiple beams connected to form the spring and multiple springs in series and parallel configurations holding the proof-mass up. Equation (4) stands for the stiffness k of a single beam, while (5) represents an approximation to the total stiffness in a spring formed by n beams of length L neglecting the length of the joints between beams and assuming the length of each beam is many times greater than the width and thickness. Finite-element analysis (FEA) results shown in Figure 3 for multi-beam spring validates (5).

$$k_{beam} = \frac{3EI}{L^3} \tag{4}$$

$$k_{spring} \approx \frac{3EI}{nL^3} \tag{5}$$

Equations (6) and (7) are the equivalent stiffness for two springs a and b connected in parallel and series configurations respectively. As seen previously in Figure 1, all four spring will work together to deliver a total stiffness k described in (8).

$$k_{a\|b} = k_a + k_b \tag{6}$$

$$k_{a-b} = \frac{k_a k_b}{k_a + k_b} \tag{7}$$

$$k = \frac{(k_1 + k_2)(k_3 + k_4)}{k_1 + k_2 + k_3 + k_4} \tag{8}$$

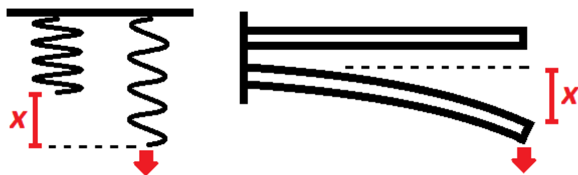

Fig. 2. Equivalent use of different kinds of spring.

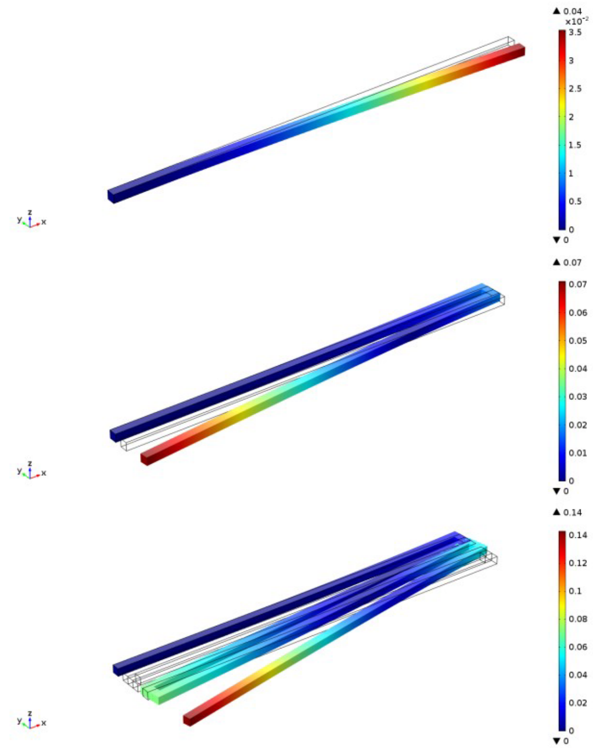

Fig. 3. FEA validation of the multi-beam spring behavior according to the number n of beams (1, 2 and 4 beams).

From (1), (3), and (8) there is a correlation between the capacitance C and the displacement of the proof-mass that is suspended by an equivalent spring of stiffness k which restoring force is opposite to the external forces accelerating the proof-mass.

II. Dynamic Model

A general expression for the proof-mass dynamics and therefore the variation in distance d separating the capacitor plates can be derived from a free-body diagram (Figure 4) and the Newton's second law. Equation (9) describes the accelerated displacement of mass m as the restoring force of the equivalent spring with stiffness k acts in opposition to an input external force $u(t)$. The Laplace transform is applied to (9) in (10) and initial conditions $x(0)$ and $\dot{x}(0)$ are assumed to be equal to zero. From the higher exponent in the denominator of transfer function (11) which is the rational relation between the displacement output and force input stimuli, we can characterize the system as one of second order.

$$m\ddot{x} = u(t) - kx$$
$$m\ddot{x} + kx - u(t) = 0 \tag{9}$$

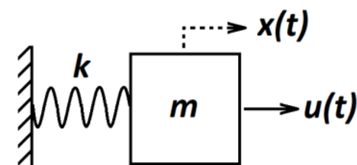

Fig. 4. Free-body diagram representing a system with mass m and a single spring with equivalent stiffness k being actuated by a force u(t).

Authorized licensed use limited to: CINVESTAV. Downloaded on August 07,2020 at 18:23:45 UTC from IEEE Xplore. Restrictions apply.

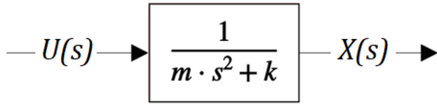

Fig. 5. Mass-spring system open-loop representation.

$$m(s^2X(s) - sx(0) - \dot{x}(0)) + kX(s) - U(s) = 0$$

$$X(s)(ms^2 + k) = U(s) \tag{10}$$

$$\frac{X(s)}{U(s)} = \frac{1}{ms^2 + k} \tag{11}$$

The open-loop representation shown in Figure 5 is sufficient to determine the response of the system to a unary step input.

III. Step and Linear Response

Neglecting gravitational and air-related friction or damping effects, as could be considered for extra-planetary aerospace applications, the step response is given by (12), where $X(s)$ is the Laplace transform of position x of the proof-mass being $x(t) = 0$ the equilibrium state of spring k, and $1/s$ the Laplace transform of unary step force input.

$$X(s) = \frac{1}{s} \cdot \frac{1}{(ms^2 + k)} \tag{12}$$

By partial-fraction decomposition a final expression (13) for $X(s)$ is obtained in the form needed to apply the inverse Laplace transform.

$$X(s) = \frac{1}{k}\left(\frac{1}{s} - \frac{s}{s^2 + \frac{k}{m}}\right) \tag{13}$$

The dynamic expression for mass m in the time domain is given by (14). This expression is general and must be put in the context of micro mechanical systems by using appropriate m and k parameters.

$$x(t) = \frac{1}{k}\left[1 - \cos\sqrt{\frac{k}{m}}t\right] \tag{14}$$

Typical dimensions for both proof-masses and springs in MEMS accelerometer designs range from 50 to 500 µm due to the size of silicon dies which are usually of 1 to 4 mm². A spring with beams 100 µm long (l_b) and 3 µm wide (w_b), and a square proof-mass with 100 µm a side, could be a good approximation to standard parameters, especially for CMOS-MEMS technology where the design space is limited as chips also contain the processing electronics and wire-bonding pad frame.

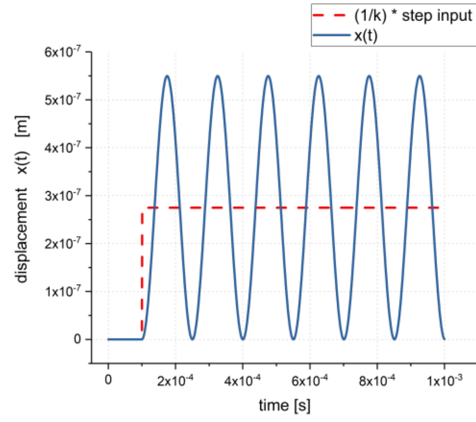

Fig. 6. Oscillatory response behavior to step input according to a mass-spring system neglecting gravity and air damping.

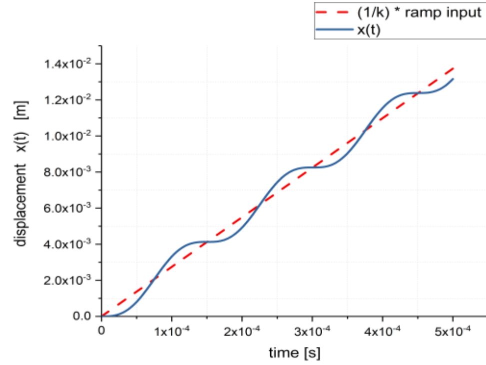

Fig. 7. Sinusoidal error signal in ramp response.

Considering aluminum structures with thickness $t = 0.77$ µm thickness of the top metal layer (Metal 3) in C5 conventional CMOS fabrication process from On-Semi [3] a 10-beam spring would have a stiffness $k =$ according to (5) and (15) where moment of inertia for a single beam is $I = tw^3/12$ and E is the Young's Modulus. Mass for the proof-mass is given by (16) where ρ is the density of aluminum and V the volume of the proof-mass.

$$k = \frac{3(70GPa)(1.7325 \times 10^{-24}m^4)}{(10)(100 \times 10^{-6}m)^3} = 0.0364\ N/m \tag{15}$$

$$m = \rho V = (2700\ kg/\mathrm{m}^3)(1 \times 10^{-4}\ \mathrm{m})^2(0.77 \times 10^{-6}\mathrm{m})$$

$$m = 2.08 \times 10^{-11}\ kg \tag{16}$$

As in (14), the dynamic expression for position $x(t)$ as a response to a linear input $u(t) = t$ (ramp) is obtained.

$$X(s) = \frac{1}{k}\left(\frac{1}{s^2} - \sqrt{\frac{m}{k}}\frac{\sqrt{\frac{k}{m}}}{s^2 + \frac{k}{m}}\right) \tag{17}$$

Authorized licensed use limited to: CINVESTAV. Downloaded on August 07,2020 at 18:23:45 UTC from IEEE Xplore. Restrictions apply.

$$x(t) = \frac{1}{k}\left(t - \sqrt{\frac{m}{k}}\sin\sqrt{\frac{k}{m}}t\right) \tag{18}$$

As can be seen in figures 6 and 7 from system simulation and in agreement with (14) and (18), a high-frequency oscillatory permanent error is present and could prevent a CMOS-MEMS device from achieving a stable output response.

This result is important to be considered especially for sensor with floating-gate-based electronics, as long as the transfer function for the capacitive voltage divider reported in [4] and [5] is one of order zero so no attenuation of high frequency components would help to filter the output signal.

IV. Air Damping Effects on Sensor's Application

As a sort of comparison with the results above, (19) is the transfer function including the damping coefficient b which according to [6] and [7] the air damping coefficient for the typical CMOS-MEMS capacitive gaps is of about $1 \times 10^{-6}\ Ns/m$ also, figures 8 and 9 that represent the air-damped response to step and ramp inputs respectively.

$$\frac{X(s)}{U(s)} = \frac{1}{ms^2 + bs + k} \tag{19}$$

As seen in Figure 8, the stationary response of the damped system to step inputs is only dependent on the total gain of the open-loops system, in the other hand the characteristic steady state error for linear input systems shown in Figure 9 will appear as long as the input signal keeps its slope, this kind of response and error can be easily determined by using a centrifuge test bench with increasing angular acceleration.

For all the models derived at this point it is important to consider that forces on the proof-mass are inertial an according to the mass m and stiffness k calculated for typical materials and dimensions, the force needed to meet displacement of about 1 micron are in the order of nano-Newtons ($1 \times 10^{-9}\ N$), this force and therefore acceleration magnitudes are considered for all the simulations in the present work.

V. Conclusion

These results suggest the necessity of air damping/resistance or any other kind of damping mechanism to be present when the traditional techniques and applications are implemented. Air- and gravity-free environments, as could be considered for some aerospace instrumentation system might require especial analysis and development procedures as long as oscillatory error could disable the operation principles in which conventional capacitive CMOS-MEMS accelerometers are based.

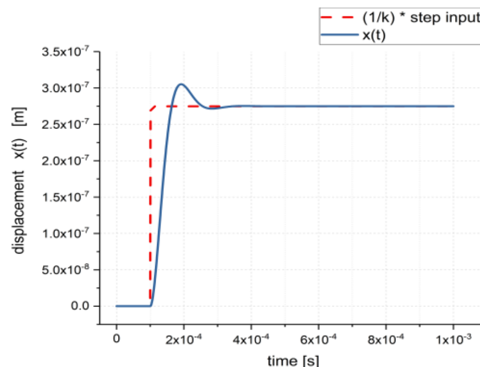

Fig. 8. Transient and steady response of an air-damped accelerometer system to a step force input.

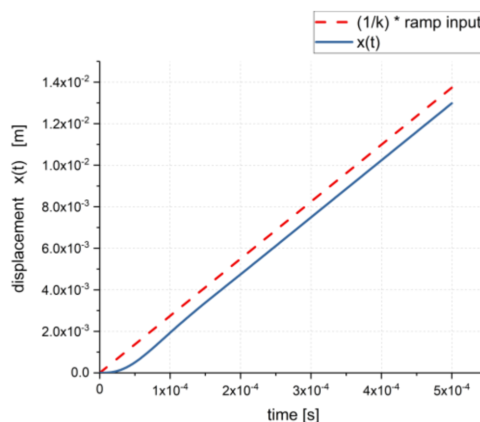

Fig. 9. Usual steady-state error in the response to a linear (ramp) input.

References

[1] B. Granados-Rojas, M. A. Reyes-Barranca, G. S. Abarca-Jiménez, L. M. Flores-Nava and J.A. Moreno-Cadena, "3-layered capacitive structure design for MEMS inertial sensing", in *2016 13th International Conference on Electrical Engineering, Computing Science and Automatic Control (CCE)*, Mexico City, Mexico, 2016.

[2] B. Granados-Rojas, M. A. Reyes-Barranca, L. M. Flores-Nava, G. S. Abarca-Jiménez, M. A. Alemán-Arce and Y. E. González-Navarro, "Composition of Metal Layers in CMOS-MEMS Micromachining Process", in *2019 16th International Conference on Electrical Engineering, Computing Science and Automatic Control (CCE)*, Mexico City, Mexico, 2019.

[3] ON Semiconductor. C5X, 0.5 Micron Technology Design Rules 4500099 Rev. X, 2011, p. 99.

[4] G. S. Abarca-Jiménez, M. A. Reyes-Barranca and S. Mendoza-Acevedo, "MEMS capacitive sensor using FGMOS", in *2013 10th International Conference on Electrical Engineering, Computing Science and Automatic Control (CCE)*, Mexico City, Mexico, 2013.

[5] G. S. Abarca-Jiménez, J. Mares-Carreño, M. A. Reyes-Barranca, B. Granados-Rojas, S. Mendoza-Acevedo, J. E. Munguía-Cervantes, and M. A. Alemán-Arce. "Inertial sensing MEMS device using a floating-gate MOS transistor as transducer by means of modifying the capacitance associated to the floating gate". *Microsystem Technologies*, 24(6), pp. 2753-2764, Jun. 2018.

[6] J. O. Dennis, A. Y. Ahmed, M. H. Md Khir and A. A. S. Rabih, "Modelling and Simulation of the Effect of Air Damping on the Frequency and Quality factor of a CMOS-MEMS Resonator". *Appl. Math. Inf. Sci. 9*, No. 2, pp. 729-737, 2015.

[7] Y. M. Mo, L. M. Du, B. B. Qu, B. Peng, J. Yang, "Damping Ratio Analysis of a Silicon Capacitive Micromechanical Accelerometer". *Wireless Sensor Network, 9*, pp. 178-188, 2017.

Authorized licensed use limited to: CINVESTAV. Downloaded on August 07,2020 at 18:23:45 UTC from IEEE Xplore. Restrictions apply.